UNIVERSITY OF OKLAHOMA

GRADUATE COLLEGE

STAND-ALONE IMAGE RECONSTRUCTION FOR MULTI-SLICE ECHO-PLANAR IMAGING, WITH APPLICATIONS TO STUDY HUMAN BRAIN FUNCTIONS

A THESIS

SUBMITTED TO THE GRADUATE FACULTY

in partial fulfillment of the requirements for the

Degree of

MASTER OF SCIENCE

IN

ELECTRICAL AND COMPUTER ENGINEERING

By

MD MEHEDI HASAN
Norman, Oklahoma
2016

STAND-ALONE IMAGE RECONSTRUCTION FOR MULTI-SLICE ECHO-PLANAR IMAGING, WITH APPLICATIONS TO STUDY HUMAN BRAIN FUNCTIONS

A THESIS APPROVED FOR THE
SCHOOL OF ELECTRICAL AND COMPUTER ENGINEERING

BY

_____
Dr. Pramode Verma, Chair

_____
Dr. Samuel Cheng

_____
Dr. Jerzy Bodurka

Table of Contents

List of Figures

Abstract

Optimizing the speed of image acquisition in magnetic resonance imaging (MRI) is a significant consideration to reduce patient examination time and/or to increase temporal resolution in dynamic studies. The advancement of simultaneous, multi-slice imaging increased the acquisition efficiency of MRI data. This technique for reducing scan time has opened a new door for functional MRI studies and diffusion-based fiber tractography to visualize the structural networks in the human brain [1]. The problem with the existing multi-slice image reconstruction algorithm using the MATLAB [2] program is that it is completely dependent on the MATLAB environment. In addition, the algorithm can be performed only on offline, preventing monitoring of subject motion and brain activation during scanning in order to adjust task presentation and for utilizing the brain signal to control other equipment and neurofeedback. To date, there is no stand-alone method for image reconstruction for multi-slice EPI data. To meet this need, I propose C/C++ programming language-based image reconstruction using the Slice-GRAPPA [3] algorithm for multi-slice acquisition and GRAPPA [4] algorithm for accelerating the image acquisition in the phase encoding direction. The main advantage of this reconstruction based on C/C++ is that it is stand-alone. In addition, optimizing the reconstruction program speed will enable it to be embedded into software to be applied in real time fMRI studies. This process was validated through matching the images from C/C++ language-based reconstruction with MATLAB environment-based reconstruction results. This thesis documents the process used to determine the efficacy of the proposed methodology.

Chapter 1: Introduction

1.1 MRI

Magnetic resonance imaging (MRI) is an imaging technique based on the principle of nuclear magnetic resonance. It is widely used in medical imaging, especially for neuroimaging due to its excellent soft tissue contrast and other range of contrast mechanisms and use of non-ionizing radiation.

The MRI device is composed of a magnet, magnetic gradient coils, a radio frequency transmitter and receiver, and a computer for controlling signal acquisition and generating MR images [5]. An MRI scanner utilizes a strong main magnetic field to polarize the protons inside the human body. In the presence of an external magnetic field, the protons undergo a precessing motion at a frequency dependent on the proton species and the strength of the magnetic field. This frequency is called the Larmor frequency. To acquire an MR signal, a radiofrequency (RF) pulse oscillating at the resonant frequency is applied, resulting in a transfer of energy in the form of photons that tip some of the protons from the low-energy (stable) to the high-energy (unstable) state. In the absence of RF pulse, the high-energy protons that were tipped return to their low-energy state to maintain equilibrium. This change in state releases energy in the form of photons, which are selected by the RF receiver coils. Thus the current that is induced in the RF coils generates the MR signal. To excite one slice at a time, gradient magnetic fields are applied in addition to main magnetic field. Because of the applied gradient field, the field strength varies with the location on which the gradient field is applied. Therefore, the precession frequencies of the protons become a function of

space, which helps to choose one slice at a time. A desired imaging slice is excited by applying an RF pulse oscillating at the slice's resonant frequency.

1.2 fMRI

Functional magnetic resonance imaging (fMRI) utilizes MRI technology to study brain functionality over time. During the fMRI experiment, several brain images are acquired while the subject performs a set of tasks. Changes in the measured signal between different images are used to make inferences regarding task-related activations in the brain. fMRI has several advantages as a brain imaging technique that includes non-invasiveness and no radiation, excellent spatial and temporal resolution and this technique is easier for the experimenter to use [11].

Blood oxygen level dependent (BOLD) contrast is used in fMRI as an indirect measure of brain neural activities [6-8]. This BOLD fMRI technique measures the ratio of oxygenated to deoxygenated hemoglobin in the blood [9]. Neural activity consumes oxygen, thereby affecting vasculature response to provide more highly oxygenated blood to local brain regions [10]. This activity results in a significant change in the amount of oxygen in the blood, indicating the extent of local neural activity. This measured signal is stated as the BOLD signal.

1.3 Echo Planar Imaging

In MRI, image data acquisition speed is one of the crucial parameters that technologists and researchers care about. Echo planar imaging (EPI) is an MR acquisition method that collects multiple segments of image data from a single spin echo or gradient echo.

It has arguably become the most talked about of MR acquisition methods because of its acquisition speed. In general, it uses a single nuclear spin excitation to obtain entire k-space data via fast switching of readout and phase-encoding gradients [12]. The capability of EPI to reduce the scan time has opened doors to a diversity of critical medical and scientific applications, such as water diffusion mapping in tissue, evaluation of cardiac function in real time, mapping of organ blood pool & perfusion, and functional imaging of the central nervous system [13].

1.4 Echo Planar Imaging Sequences

The echo planar imaging technique uses the transverse magnetization by producing a series of gradient echoes that uses a bipolar oscillating readout gradient before the transverse magnetization decays due to T2* relaxation. In between each echo readout, phase encoding blips are played to encode multiple k-space lines with a single RF excitation. Following an RF excitation, the number of gradient echoes generated is defined as *echo train length* (or ETL). The scan-time reduction factor in EPI pulse directly depends on echo train length sequences and has a significant effect on artifacts generated with EPI such as image distortion, signal loss, chemical shift displacement, and image blurring.

1.4.1 Gradient Echo EPI

A generalized gradient echo EPI sequence is shown in Fig. 1. To produce the FID (fast induction decay) signal, the pulse sequence starts with a slice selective excitation like the standard gradient echo. A series of spatially encoded gradient echoes are produced using a train of bipolar readout gradient that oscillates rapidly from positive to negative amplitude and phase-encoding gradient blips under the envelope of FID [14].

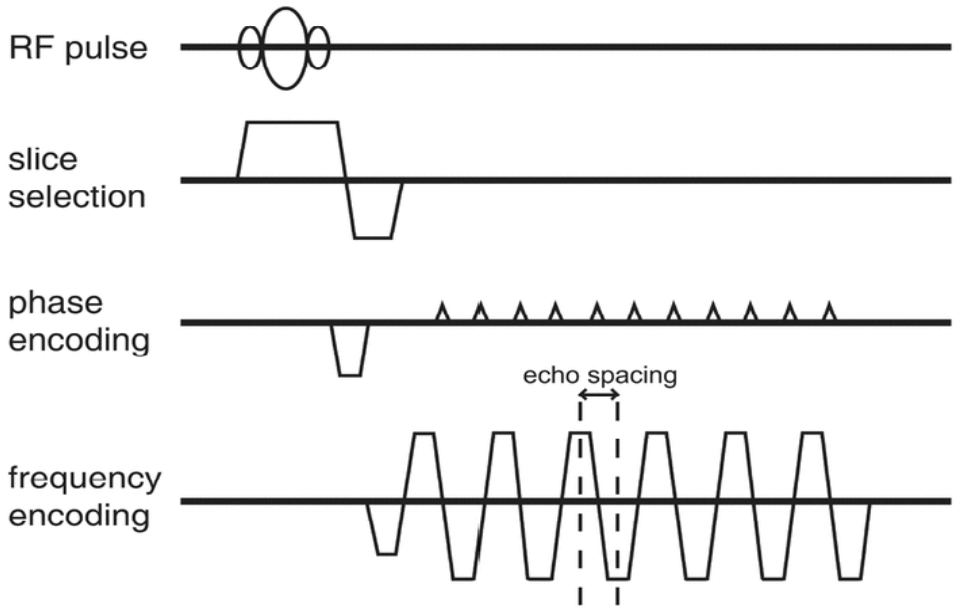

Figure 1: Gradient echo EPI sequence. The interval between two successive echoes can be defined as echo spacing [15]

Along the phase-encoding direction, every k-space line is acquired at a different echo time (TE). The gradient echo amplitude S(n) decays for the corresponding echo time can be expressed by the following equation.

$$S(n)=S_0 + e^{\frac{-TE(n)}{T2*}} \quad (1)$$

Here, *n* denotes the echo index in the echo train and S_0 represents the signal at time zero, which can be defined as the time instantly after the magnetization is tipped by the used RF pulse.

The gradient echo EPI sequence is used for numerous reasons. The most important reason is to capture functional imaging. The contrast behavior includes a T2* instead of a T2 component due to local field inhomogeneities. As a result, the signal intensity decays after excitation at a rate determined by local field inhomogeneities [16]. With gradient echo EPI, it is also possible to use shorter TRs without suffering large signal losses because the smaller excitation flip angle results in fewer disturbances from magnetic equilibrium and, therefore, shorter relaxation recovery times [16].

1.4.2 Spin Echo EPI

Spin echo EPI depends on gradient echoes sampling k-space similar to gradient echo EPI, except that instead of free induction decay, the gradient echoes are generated under the spin echo [17]. Fig. 4 shows the generalized spin echo EPI sequence. In this case, the spatial encoding *module* is preceded by a 90° excitation pulse and a 180° echo-forming pulse that results in the formation of a Hahn echo [17] during the readout period. The signal intensity (SI) of the image can be described by the following equation [16]:

$$SI=k\rho(1 - e^{-Tr/T1})\, e^{-Te/T2} \quad (2)$$

Here, k is the sequence independent factors such as magnetic field strength and RF denotes the "echo time" or the time between excitation pulse and center of the *r* coil

sensitivity, *p* is the tissue proton density, T_r denotes the repetition and T_e readout period. SE-EPI images show relatively little sensitivity to local field inhomogeneities and behave similarly to conventionally acquired MR images. The major difference is that in a single shot EPI case, the images are obtained with little or no T_1 contrast since the repetition time is effectively infinite [16]. This is a great advantage in T_2-weighted studies where the T_1 and T_2 contrast mechanisms when put together, the overall image contrast is reduced [16].

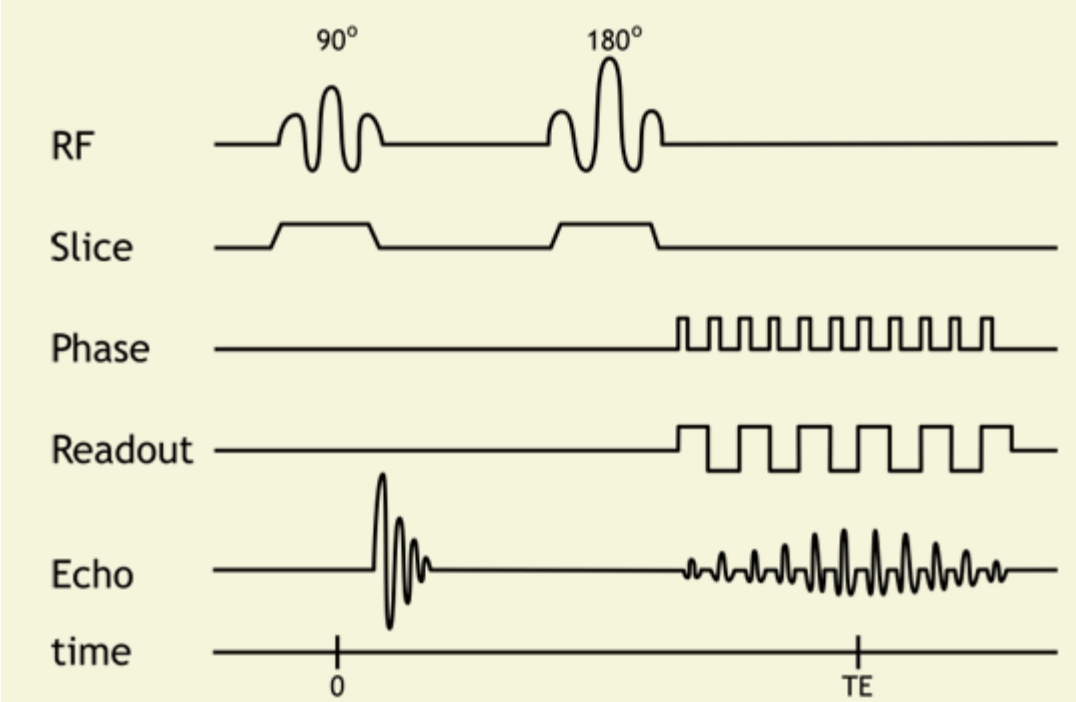

Figure 2: Pulse sequence diagram for spin echo EPI. Here, within a spin echo multiple gradient echoes are formed [18]

1.4.3 Inversion Recovery EPI

In inversion recovery EPI (IR-EPI), an inversion recovery module is generated earlier to a GE-EPI or SE-EPI pulse sequence. Fig. 3 shows the generalized inversion recovery EPI sequence.

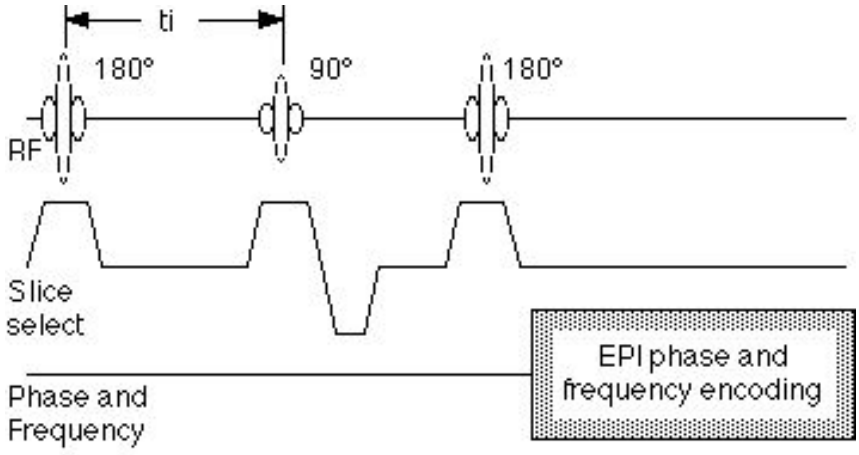

Figure 3: Pulse sequence diagram for inversion recovery EPI. Due to the added 180° RF pulse prior to standard spin echo EPI scan results in inversion-recovery contrast behavior [16]

Inversion recovery EPI has various usages, which include measuring tissue perfusion with arterial spin labeling (ASL). This pulse sequence is also used to form a desired tissue contrast as in magnetization-prepared, T1-weighted imaging to reduce the signal from cerebrospinal fluid or to produce a T1 map.

1.5 Organization of the Thesis

In this thesis introduces a C/C++ based, stand-alone image reconstruction for multi-slice echo planar imaging. The rest of the thesis is organized as follows. Chapter 2 describes reducing the scan time and different parallel imaging approaches for reducing the scan time in the phase encoding direction. It also discusses the multi-slice imaging approach and different parallel imaging-based algorithm for acquisition of simultaneous

multi-slice echo planar imaging. Chapter 3 presents problems associated with acquiring different multi-slice data, briefly describes the blipped-CAIPIRINHA method for simultaneous multi-slice acquisition, and justifies the advantage of using the method. Chapter 3 also discusses the slice-GRAPPA method in detail, which is followed to reconstruct the simultaneously acquired, multi-slice images. Chapter 4 discusses the results acquired from the C/C++ based, stand-alone reconstruction. Chapter 5 draws some conclusions for the proposed work and offers suggestions for improving the proposed work.

Chapter 2: Methods to Reduce the Scan Time

In general, there are several ways to reduce the scan time in MRI. One of them is to fully sample k-space at a faster rate than the usual using the fast imaging sequences. Another approach includes acquiring partially sample k-space data to increase the speed of image acquisition where the missing information can be calculated using the parallel imaging techniques. Finally, simultaneously excited multi-slice acquisition approach can decrease the MRI imaging time.

2.1 Parallel Imaging

Parallel magnetic resonance imaging is a robust method for accelerating conventional MRI encoding. It works by acquiring a reduced amount of k-space data, using an array of receiver coils with spatially varying sensitivities. This array of receiver coils can be used to calculate the missing data as well as the consequent aliasing in the image.

2.2 Basic Concepts of Parallel Imaging

2.2.1 K-space and the MR Image

In MRI, the data are collected in k-space. The k-space data are collected by varying the magnetic field strength in a particular direction. Once all the data are collected, the inverse Fourier transform is taken to acquire the whole image [20]. The k-space point space in each direction is inversely proportional to the field of view (FOV). So, decreasing the k-space point space increases the field of view. In other

words, the more k-space points in one direction, the larger the field of view in that direction.

$$FOV_X = \frac{1}{\Delta Kx} = \text{sampling rate along } K_X$$

$$FOV_y = \frac{1}{\Delta Ky} = \text{sampling rate along } K_y \quad (3)$$

On the other hand, spatial resolution depends on the width of the k-space coverage. That means the highest frequency collected in the k-space (k_{xmax} or k_{ymax}) is inversely proportional to the image resolution. As a result, increasing k_{ymax} results in decreasing the Δy and increasing the image resolution in the y direction.

$$\delta_x \approx \frac{1}{2Kxmax}$$

$$\delta_y \approx \frac{1}{2Kymax} \quad (4)$$

K-space data are generally collected line by line to fill a grid of points. Generally kx direction is considered the readout direction, and the ky direction is the phase-encoding direction. In a 3-D scan, the k_z direction corresponds to the partition encoding direction [20]. The total acquisition (T_A) time for a 2D dataset is calculated using the following equation:

$$T_A = T_R \times N_{PE} \quad (5)$$

Here, T_R is the repetition time, or the time from the application of an excitation pulse to the application of the next pulse along the k_x direction. N_{PE} is the total number of phase encoding lines in the k_y direction.

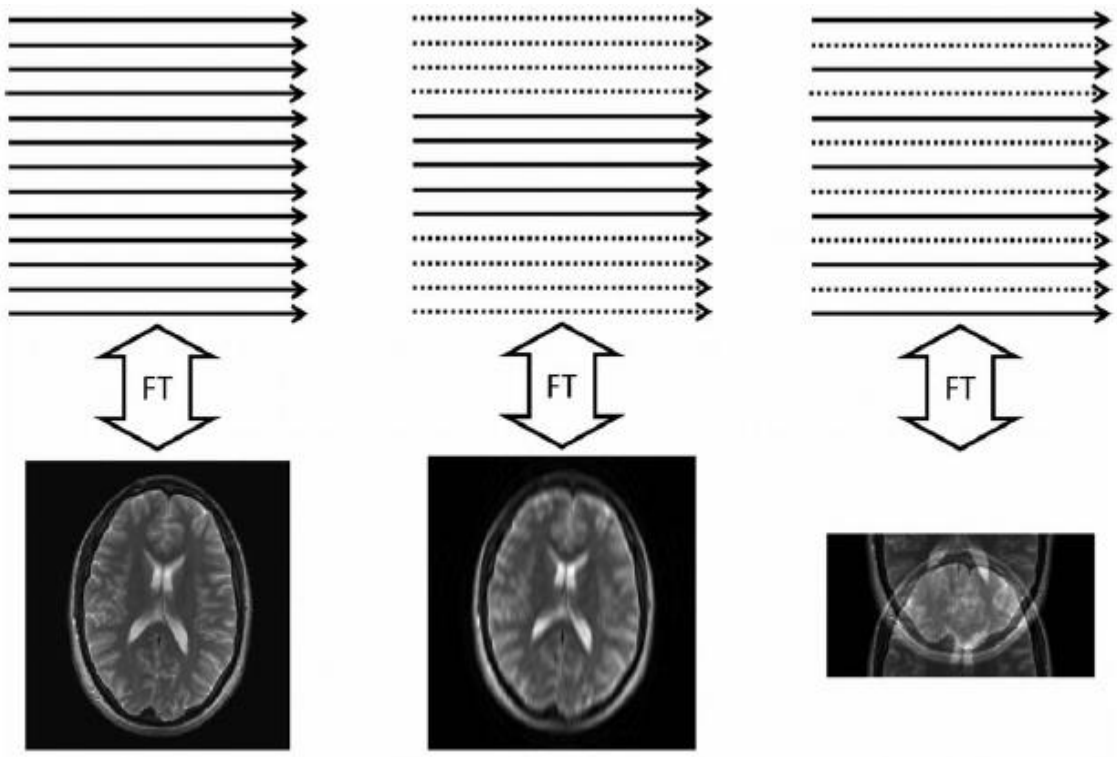

(a) **(b)** **(c)**

Figure 4: (a): Big Kymax and small Δky spacing results in full FOV and full resolution. (b): Reduced Kymax with small Δky spacing results in lower resolution while maintaining the full FOV (c): Increased Δky with big Kymax results in decreased FOV [20]

To reduce the scan time, T_R or N_{PE} must be reduced. In order to reduce $T_{R,}$ the k-space data should be collected more quickly than the usual. K-space data collection speed depends on the desired image contrast and the strength of the magnetic field gradient required encoding the k-space data. For some types of scan, T_R needed to be long in order to achieve the desired image contrast. Hence the TR cannot be short. In other types of scan, to keep the T_R short, rapidly switching high-strength magnetic field gradients are needed. Hence, the electrical power required would be high. Moreover, the rapidly switching high-strength magnetic field gradients could induce electrical currents in the patient, potentially causing the peripheral nerve simulation [21-23]. In addition,

when using some fast multi-echo pulse sequences at high magnetic field strength, the specific absorption rate can limit the minimum achievable T_R that, in turn, will limit the speed at which data can be acquired [24]. The other method to decrease the T_A is to reduce the N_{PE} in the equation that is decreasing the amount of k-space data collected. It can be achieved by either decreasing the k_{ymax} or by removing some phase encoding lines. Because decreasing the k_{ymax} will lead to a reduction in image resolution, spacing between k-space in the y direction is increased to speed the acquisition of MRI data. However, this action result in smaller FOV, hence spatial aliasing. Fig. 4 shows the case for reduced k_{ymax} (Fig. 4 (b)), increased Δk_y (Fig. 4 (c)). But the aliasing image could be separated using different parallel imaging methods, which will be discussed in the next section.

2.2.2 Coil Array

In parallel magnetic resonance imaging, the signal is obtained using an array of receiver coils with different spatial sensitivities. A single receiver channel in an array is sensitive to signals generated from a specific spatial region, which can be seen in Fig. 4. The signal S_n received by the *n*th receiver from the coil array for an ideal receiver array is the following:

$$S_n(x,y)=S(x,y)\, C_n(x,y) \tag{6}$$

where $C_n(x,y)$ is the sensitivity of the *n*th receiver coil, and $S(x,y)$ is the signal received by the coil with homogeneous receive sensitivity.

In the array, this individual coils are organized so that the sensitivity profiles cover the desired FOV (Fig. 5). When a scan is performed, all of the images resulting

from the several channels must be combined to form a single image. This combination can be done by means of a sum-of-squares operation [25] or using other methods that result in a homogeneous signal after the combination [26].

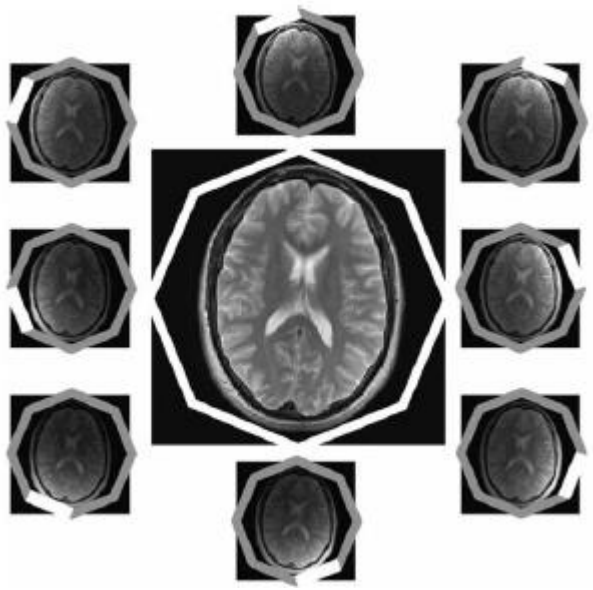

Figure 5: An example of head coil array that is made up of eight independent receiver coils arranged around the object in a circle. The combined magnitude image is shown in the center [20]

2.3 Parallel Imaging Techniques

There are two approaches to reconstructing the image in parallel imaging methods: image-based and k-space based. Image-based methods reconstruct images from each coil element with reduced FOV and then combining the images using knowledge of individual coil sensitivities (SENSE). On the other hand, k-space-based methods explicitly calculate the missing k-space lines before Fourier transformation of the raw data is performed (SMASH, GRAPPA).

2.3.1 SENSE (Sensitivity Encoding)

The SENSE parallel imaging reconstruction method [27] is characterized as an image domain *unfolding* algorithm [28]. In the Cartesian-type sampled k-space, the location of and distance between periodic recurrences in the image domain are well known [28]. A parallel imaging accelerated acquisition with a reduction factor R results in a reduced FOV in every component coil image. A schematic example of the SENSE method using a four-channel linear array is shown in Fig. 6 where the acceleration factor R=2.

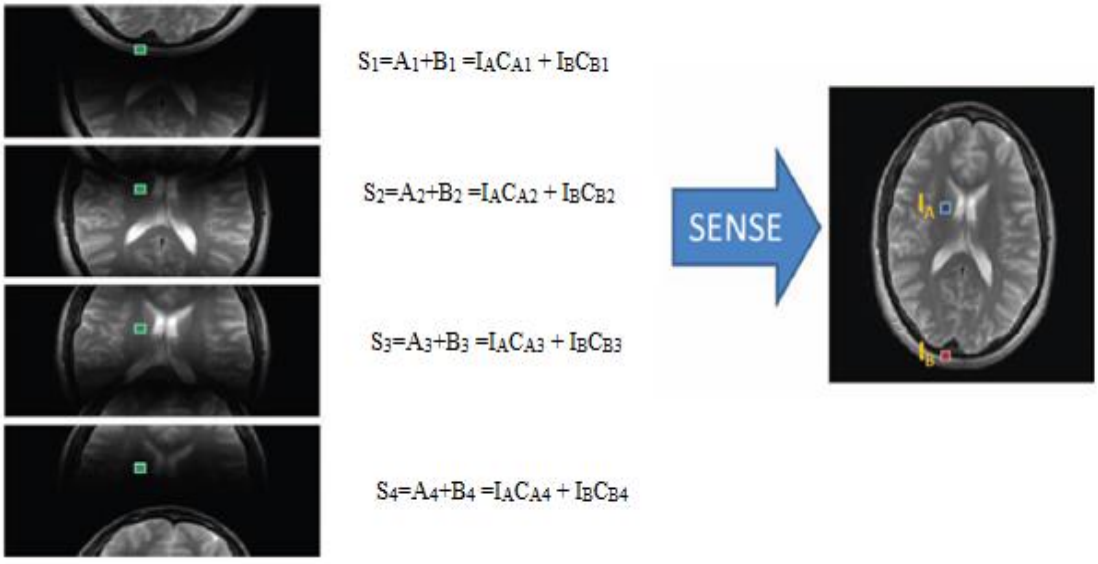

Figure 6: For an acceleration factor R=2, a four channel linear array is used. Four single coil images were formed where pixels IA and IB aliased on each other. The SENSE algorithm is used to unfold the aliased single-coil images into a full FOV image [20]

In this case, FOV has been reduced to one-half the results in aliasing of two pixels on top of each other in each of the single channel images. However, these pixels

are multiplied by the suitable coil sensitivity value and then added together in the aliased image. This function is shown in the following equation:

$$\begin{aligned} S_1 &= A_1 + B_1 = I_A C_{A1} + I_B C_{B1} \\ S_2 &= A_2 + B_2 = I_A C_{A2} + I_B C_{B2} \\ S_3 &= A_3 + B_3 = I_A C_{A3} + I_B C_{B3} \\ S_4 &= A_4 + B_4 = I_A C_{A4} + I_B C_{B4} \end{aligned} \tag{7}$$

Here, S denotes the aliased pixel, C denotes the coil sensitivities, and I represents the values of the pixels in the desired image at locations A and B. From (7) if the coil sensitivity value C is known and the aliased pixel value S is known, there are only two unknown values I_A and I_B remaining, which can easily be solved using (7). The above equation from (7) can be written in matrix form as:

$$S = IC \tag{8}$$

where C is a matrix with a size NXR (N = number of coils and R = acceleration factor). The system of equations from (7) can be solved for the case $N \geq R$. Though for simplicity, only four coil arrays are considered in the discussion here. In general larger number of coils are used in an array for image acquisition [13].

2.3.2 SMASH

The basic concept used in simultaneous acquisition of spatial harmonics (SMASH) algorithm [29] is that missing phase-encoding steps can be generated directly from a linear combination of the individual coil sensitivities of the receiver array. A schematic illustration of SMASH algorithm is shown in Fig. 7

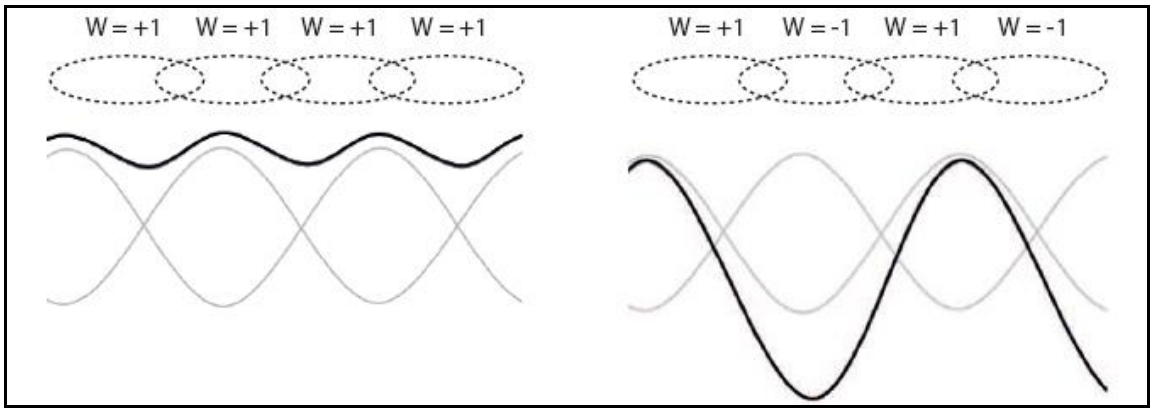

Figure 7: A schematic illustration of combining coil sensitivities with appropriate linear weights to produce composite sensitivity as is done for SMASH reconstruction [13]

In SMASH, combining the coil sensitivity values $C_k(x,y)$ with appropriate linear weights $n_k^{(m)}$ produce composite sensitivity profiles C_m^{comp} that include sinusoidal spatial sensitivity variations of the order m as represented by the following equation:

$$C_m^{comp}(x,y)=\sum_{k=1}^{Nc} n_k^{(m)} C_k(x,y) \cong e^{im\Delta kyY} \quad (9)$$

where, $\Delta ky=2\pi/FOV$ and N_C is the number of coil elements in an array coil. Integer m specifies the order of the generated spatial harmonic. The only unknowns in (9) are the linear weights $n_k^{(m)}$, which can be estimated by fitting (e.g., least square fit) the coil sensitivity profiles C_k to the spatial harmonic of order m. The component coil signal $S_k(ky)$ in the phase-encoding direction is received in coil k and can be calculated as the Fourier transform of the spin density $\rho(y)$ fitted with the coil sensitivity profile $C_K(y)$:

$$S_K(k_y) = \int \rho(y)\, e^{ikyY} dy \quad (10)$$

Using (9) and (10), it is possible to derive an expression to generate shifted *k*-space lines $S(k_y + m\Delta k_y)$ from weighted combinations of measured component coil signals $Sk\ (ky)$. The expression is shown below:

$$\sum_{k=1}^{N_c} n_k^{(m)} . S_k(k_y) = \int (y) \sum_{k=1}^{N_c} n_k^{(m)} C_k(y) e^{ik_y y} dy$$

$$= \int (y) e^{im\Delta k_y y} e^{ik_y y} dy$$

$$= S^{comp}(k_y + m\Delta k_y) \qquad (11)$$

Equation 11 represents the fundamental SMASH relation and specifies that linear combinations of component coils can be used to generate missing k-space lines from adjacent acquired k-space lines. In general, although this approach is applicable only if the coils are arranged in a linear fashion in an array, it is able to generate the preferred spatial harmonics in phase-encoding direction with adequate accuracy.

2.3.3 AUTO-SMASH and VD-AUTO-SMASH

In AUTO-SMASH, the component coil sensitivities are estimated by acquiring a small number of additional fully sampled central k-space regions, known as auto-calibration signals (ACS), with the under-sampled k-space data [30]. Fig. 8(b) shows an AUTO-SMASH-type acquisition scheme for a reduction factor R=3. In general, R-1 extra ACS line is acquired in the center of k-space at locations mΔky, where m counts from 1 to R-1 [32]. These additionally obtained ACS lines S_k^{ACS} are used to derive the linear weights $n_k^{(m)}$ that are required to generate the missing k-space lines. The

component coil images that correspond to k-space shift of mΔky should be equal to the weighted combination of auto-calibration profile obtained at ky + mΔky.

$$S^{comp}(k_y+m\Delta k_y) = \sum_{k=1}^{N_c} S_k^{ACS}(k_y+m\Delta k_y)$$

$$\cong \sum_{k=1}^{N_c} n_k^{(m)} S_k(k_y) \qquad (12)$$

By solving (12), a set of linear weights $\mathbf{n_k^{(m)}}$ can be derived, which can be used to generate the missing k-space lines. Once all the missing k-space lines are generated in an under-sampled k-space data, a full FOV image can be generated by applying the inverse Fourier transformation.

To further improve the reconstruction procedure of the AUTO-SMASH approach the idea of variable-density, (VD)-AUTO-SMASH was introduced. In the VD-AUTO-SMASH approach (Fig. 8(c)) [31], the number of available fits to derive the weights $\mathbf{n_k^{(m)}}$ for the desired k-space shifts (m=+1,-1) are significantly increased by acquiring multiple ACS lines instead of only R-1 number of lines. To further improve the image reconstruction quality, these reference data can be integrated with final k-space data, thus partially replacing generated k-space lines by actually acquired k-space lines.

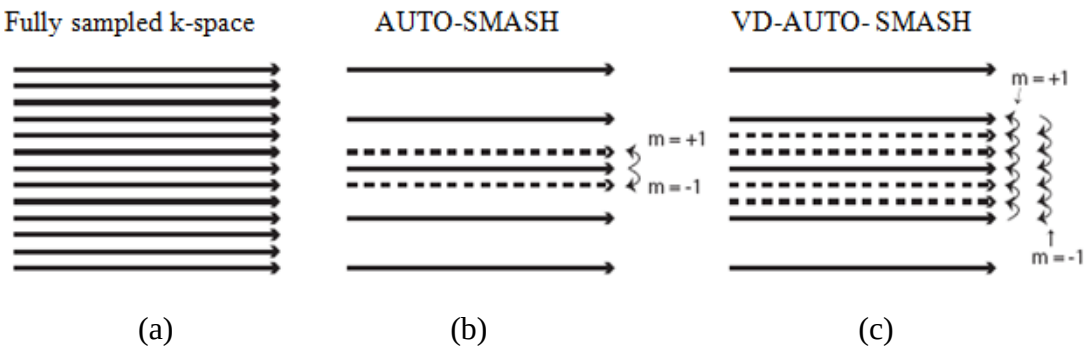

Figure 8: (a) A fully Fourier encoded k-space is shown (b) In this example for R=3, in AUTO-SMASH, the central 2 auto-calibration lines are additionally acquired (c) In VD-AUTO-SMASH, multiple auto-calibration lines are obtained.

2.3.4 GRAPPA (Generalized Autocalibrating Partially Parallel Acquisition)

GRAPPA is basically a more generalized implementation of the VD-AUTO-SMASH approach. Although both techniques follow the same acquisition procedure, they differ considerably in the way reconstruction of missing k-space lines is calculated. In GRAPPA, multiple blockwise reconstructions are performed to generate the missing k-space line for each of the coil that results in uncombined images for each coil in the array [4]. Fig. 8 shows the schematic diagram of the GRAPPA algorithm. Multiple lines from all the coils are used to fit an ACS line in a single coil. In Fig. 9, four lines are used from all four coils to fit an ACS line from coil 4. This fit provides the linear weight used to generate the missing k-space line for that coil. Once all the k-space lines are generated for a particular coil, a Fourier transform is performed to synthesize the uncombined image for that coil. This process is repeated for each of the coils of the array, resulting in a full set of uncombined images for every coil in the array.

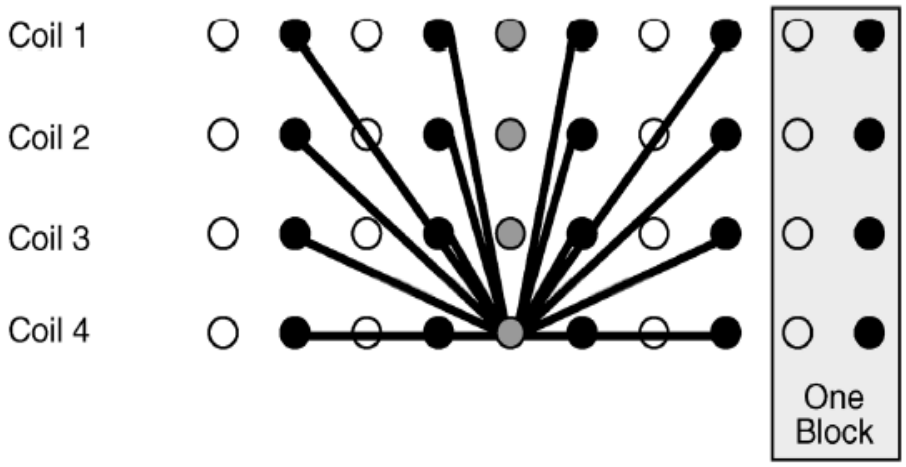

Figure 9: The GRAPPA algorithm is shown for four coils array for an acceleration factor of two. On the right side a block is shown which is defined as a single acquired line plus the missing k-space lines next to that line [4]

The individual coil images are then combined into a composite image using a normal sum of squares reconstruction [33]. In general, the above mentioned process of reconstructing the missing data in coil j at a line (k_y -mΔk_y) offset from the normally obtained data using a blockwise reconstruction is represented by the following equation:

$$S_j(k_y - m\Delta k_y) = \sum_{l=1}^{L} \sum_{b=0}^{Nb-1} n(j,b,l,m)\, S_j(k_y - bA\Delta k_y) \qquad (13)$$

where A denotes the acceleration factor, N_b represents the number of blocks used in the reconstruction where a block can be defined as a single acquired k-space line and (A -1) missing lines; n(j,b,l,m) represents the linear weights in the linear combination. The index l counts from 1 to L for l element coil array, and the index b counts through the individual reconstruction blocks. This procedure is repeated and full k-spaces are derived for each coil in the array. This results in L uncombined single coil images, which can be combined finally to a single image using a conventional sum of squares reconstruction [34] or any other optimal array combination [35].

The original implementation of GRAPPA approach was later improved by including the points along the k_x direction in the kernel used to determine the coil weights [13]. Since GRAPPA method does not depend on the exact knowledge of the coil sensitivities, it provides more accurate images in cases where it might be difficult to obtain coil sensitivity map such as in regions that are subject to patient motion and images with areas of low signal. In addition, GRAPPA can sometimes provide images with fewer artifacts when there is aliasing in the full FOV image [36-37].

2.4 SNR and Geometry Factor (g) in parallel imaging

In general, Parallel imaging approach suffers from an SNR loss by a factor of $\sqrt{R}$ due to reduced Fourier averaging. Moreover, the SNR of reconstructed images depends on how different the coil sensitivities are at the location of the aliased pixels. Therefore, an additional term, called the geometry factor or g-factor [38], needs to be taken into account to compare SNR of images obtained with parallel imaging. As a result, the SNR of the final image acquired with parallel imaging approach can be shown as following.

$$SNR_{PI} = \frac{SNR}{\sqrt{R}.g} \tag{14}$$

Where, SNR_{PI} denotes the SNR of images acquired with parallel imaging, SNR denotes the SNR of fully sampled images. R is the reduction factor, and g is geometry factor. SENSE g-factor is derived from explicit knowledge of the coil sensitivity profiles. On other hand, the GRAPPA g-factor is calculated using the GRAPPA

weights. Although the GRAPPA g-factor and SENSE g-factor differ because the techniques are not the same, still they likely to be quite similar as the g-factor originates from the coil sensitivities for both approaches.

2.5 Simultaneous Multi-Slice Acquisition (SMS Acquisition)

For dynamic studies of the brain, such as diffusion-weighted imaging or functional MRI, the speed of acquiring the images is of utmost importance. Although conventional parallel imaging approaches can greatly reduce the scan time by eliminating phase encoding steps, it does not significantly reduce TR or acquisition time for diffusion and fMRI sequence since it contains large, fixed time blocks that cannot be shortened for action such as for a suitable echo time (TE) for T2* contrast. On the other hand, simultaneous multi-slice acquisition accelerates the acquisition by acquiring multiple slices together instead of just a single slice. Moreover, unlike conventional parallel imaging acceleration, since SMS acquisition does not shorten the readout period or omit k-space samples, it is not subject to a $\sqrt{R}$ penalty on SNR. Simultaneous multi-slice imaging technique undersamples data in the slice direction and the slice images are unfolded using the algorithm of conventional parallel imaging methods. Figure 10 (a) and (b) shows the difference between the conventional acquisition (10(a)) and multi slice acquisition (10(b)).

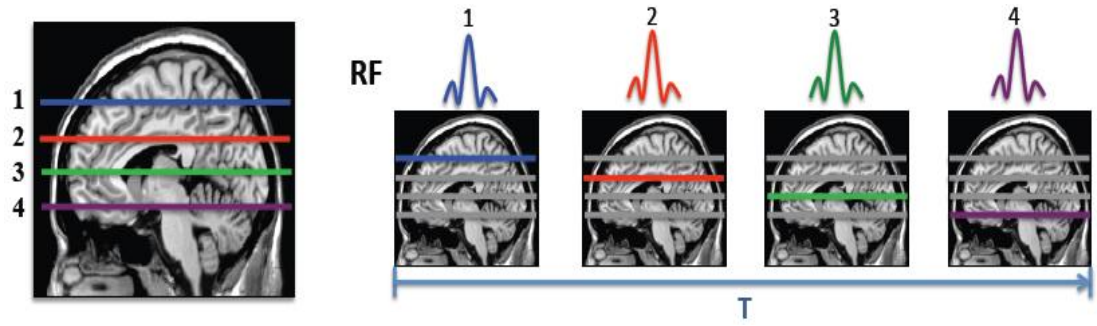

(a) Conventional Imaging

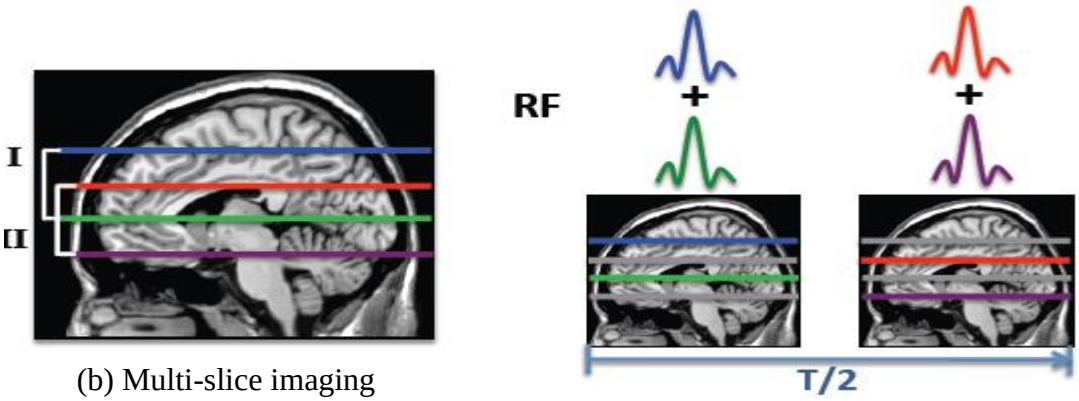

(b) Multi-slice imaging

Figure 10: (a) Conventional image acquisition where one slice is acquired per shot. (b) multi-slice acquisition where two slice is acquired per shot decreasing the total acquisition time directly by a factor of two.

2.6 Simultaneous Multi-Slice Acquisition (SMS Acquisition) Techniques

2.6.1 SENSE algorithm for SMS acquisition

Simultaneously multi-slice acquisition was first demonstrated by Larkman et al. [39] who proposed to use the SENSE (Sensitivity Encoding) algorithm, in other words, information from sensitivity profile of the RF coils to reconstruct the slice image [40]. This method for separating the slices works if there is at least the same number of coils as slices and complex sensitivity varies for each coil to any given slice. The complex signal acquired in coil j in a single pixel (S_j) is represented by the following equation:

$$S_j = I_{j1}C_{j1} + I_{j2}C_{j2} + \ldots.. + I_{jk}C_{jk} \quad (15)$$

where C_{jk} is the complex sensitivity of coil j at spatial location k for multi-slice and I_k denotes the spatially dependent complex signal from slice j. An equation can be derived from (15) and can be written in matrix form as:

$$[S]=[I][C] \tag{16}$$

The solution for [I] is given by:

$$[I]=[S]^{-1} . [C] \tag{17}$$

where $[S]^{-1}$ denotes the inverse of the complex sensitivity matrix.

2.6.2 SENSE/GRAPPA Algorithm for SMS Acquisition

While the SENSE algorithm for multiband imaging aims to unfold the aliased slices in the image domain, an alternate method for generating missing data was proposed. It is a combination of SESNE and GRAPPA [41]. In the SENSE/GRAPPA combination method, both in-plane acceleration and slice direction acceleration is considered. Fig. 11 illustrates the basic SENSE/GRAPPA technique. The fitting equation of the SENSE/GRAPPA kernel is given by the following equation:

$$\hat{S}_j(K_x,\hat{K}_y-m\Delta\hat{K}_y) = \sum_{l=1}^{L} \sum_{b_x=-B_x}^{B_x} \sum_{b_{xy}=-B_y}^{B_y} n_{j,m,l}^{b_x,b_y} \hat{S}_l(K_x-b_x\Delta K_x,\hat{K}_y-b_y N_{slice}\Delta\hat{K}_y) \tag{18}$$

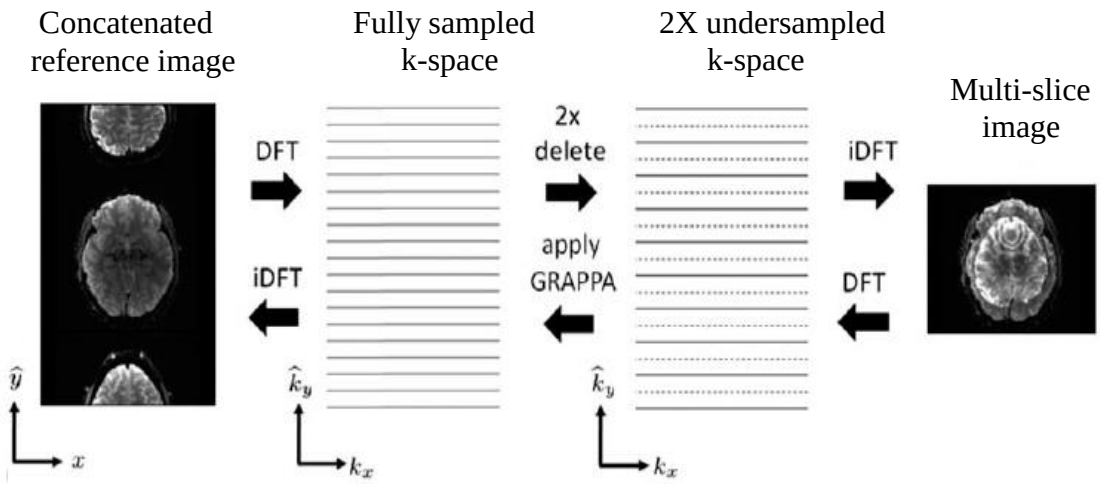

Figure 11: In the SENSE/GRAPPA algorithm where an undersampled concatenated image's k-space data results in a slice-collapsed image and, conversely, application of the GRAPPA operator to the aliased data generates a concatenated but un-aliased version of the two [3]

2.6.3 Slice-GRAPPA Algorithm for SMS Acquisition

The Slice-GRAPPA algorithm was introduced by Setsompop et al. [3] to overcome the issue of significant aliasing artifact associated with SENSE/GRAPPA method. This Slice-GRAPPA approach is developed based on the k-space base parallel imaging method used in GRAPPA. In slice-GRAPPA algorithm, before the scan, calibration data set are acquired for each slice one slice at a time. These prescan GRAPPA kernels are fitted and applied to the simultaneously acquired multi-slice to generate the missing k-space data. Once all the k-space data are generated for each slice, the inverse Fourier transform is performed to acquire the corresponding image. This slice-GRAPPA algorithm is followed in this proposed stand-alone reconstruction for multi-slice EPI images. The details of slice-GRAPPA algorithm are described in chapter 3.

Chapter 3: Methodology

3.1 Problems Associated with Different Multi-slice Approaches

Various methods have been proposed for acquisition of simultaneous multiplanar imaging. Echo volumar imaging and its variants [42, 43-46]) re single–shot, simultaneous, multiplanar imging methods. Echo volumar imaging and its variants offer the benefits of true Fourier-encoded, 3D, single-shot imaging. However it has the limitation of susceptibility distortions in the slowly encoded k-space direction. It also has the trouble of performing the entire 3D trajectory within the T2 * decay time [setsompop]. Thus, echo volumar imaging requires considerable parallel imaging acceleration to mitigate these concerns [46].

Various multi-slice methods using slice selection to excite multiple slices simultaneously exists. Wideband imaging technique (47-49) applies a slice gradient (Gz) during the readout gradient (Gx) to isolate the slices in the frequency. Although it presents a simple way to disentangle the slice information, the simultaneous readout and slice gradients create an unwanted ‘‘voxel tilting’’ effect, whereby the readout and slice direction are no longer orthogonal [3]. Simultaneous echo refocusing (SER) [50] or simultaneous image refocused [51] uses serial excitation of the imaging slices followed by a shared EPI readout. But this procedure makes the readout period long and. as a result, the total echo train length increases the susceptibility-related image distortion in EPI [3].

A second class of simultaneous multi-slice methods uses parallel image reconstruction based multi-slice imaging to un-alias the pixels from slices excited and

encoded simultaneously [52-55]. The problem associated with the parallel imaging method is that the aliased slices are generally close to each other due to a relatively smaller FOV in the slice direction. Due to the short distances between aliased pixels, it creates a great demand on the spatial variations in the coil sensitivities and results in unaliasing artifacts and a high g-factor penalty [3].

3.2 Blipped CAIPI Approach

The target of the blipped-CAIPI technique is to achieve the same interslice image shift like the blipped-wideband technique but without the unwanted blurring/tilting artifact. In order to achieve this, G_z blips are modified, resulting in their imparting the preferred phase modulation along ky without causing major phase accrual over the EPI readout period. In Fig. 12(b-d), this can be observed clearly. Fig. 12(b) shows that the phase-cycled G_z blips now exhibit a sign reversal on every other PE line. The desired phase increment is still achieved for the corresponding phase evolution at the center of the top slice. The corresponding phase evolution at the center of the top slice still exhibits the desired phase increment. Now, the incremental phases at the slice edges no longer accrue over the readout period, since sign modulation of the G_z blips exists. They move back and forth between two small amplitude conditions, and $A_{prewind}$ is chosen to balance these states so they are centered on zero. From Fig. 12(c), one can see that the phase variation within the excited slices is $\pm\delta/2$ with the same magnitude of variation. So, the following equation can be written:

$$\theta(z', \mathrm{Ny}) = (-1)^{\mathrm{Ny}+1}\gamma A_{blip}\, z'/2 \tag{19}$$

As a result, the signal attenuation is same for all k_y lines that results in a flat attenuation plot as shown in Fig 12(c) and no filtering effect, and thus a preserved spatial point-spread function. Fig. 12(d) shows resulting spatial point-spread function shows, which is an ideal delta function for all z positions within the slice. But the phase differences between even and odd lines results in some FOV/2 ghosting. The ghosting within each slice varies linearly as a function of z, considering no variation in the underlying signal within the slice; the ghosting will cancel for the summed signal along the slice direction.

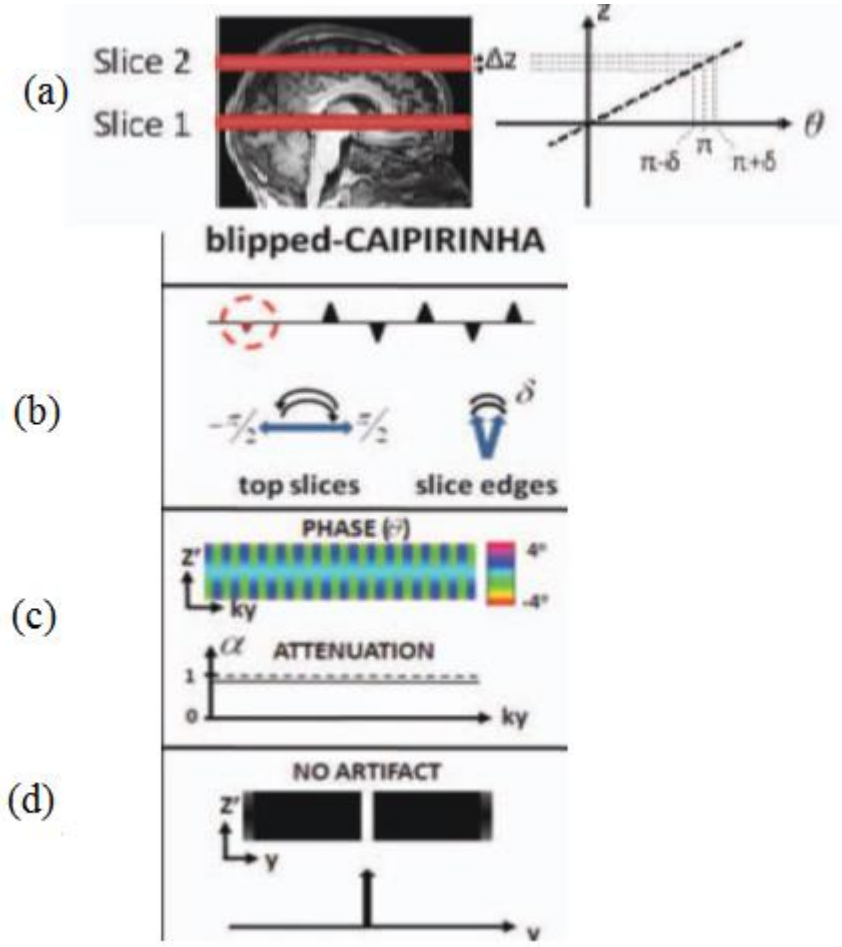

Figure 12: blipped-CAIPI method. (a) Two simultaneously excited slices (b) Gz and phase diagrams (c) Fourier space artifact (d) Spatial point-spread function (ABS) [3]

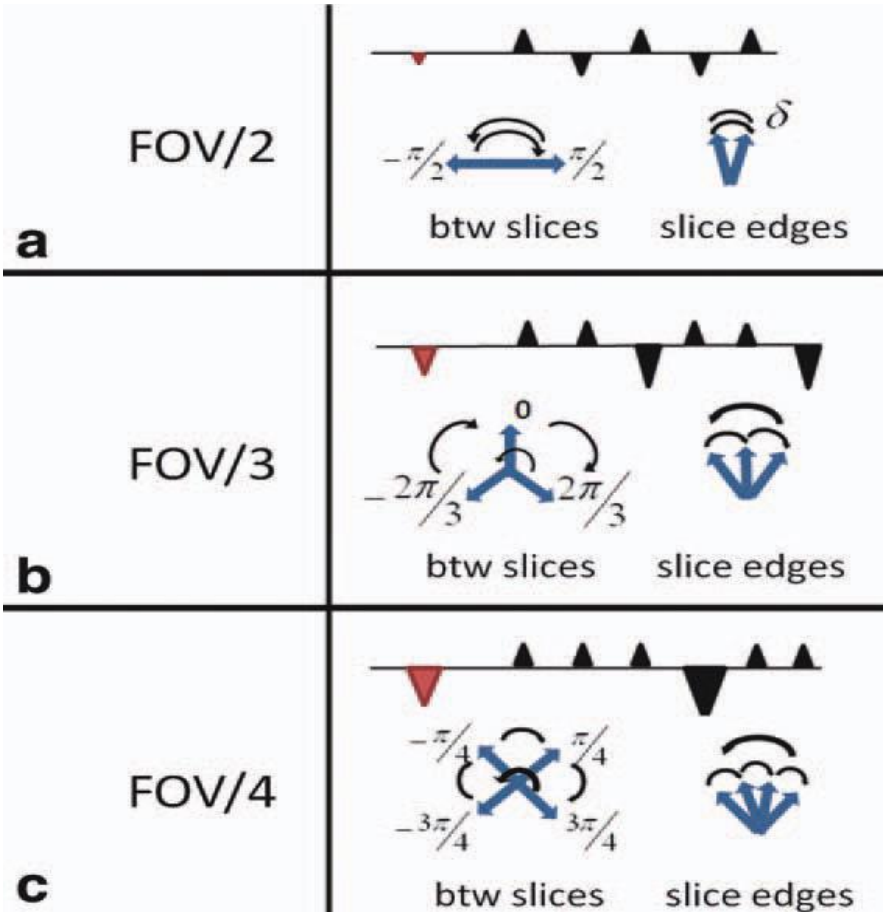

Figure 13: Generalized blipped-CAIPI method for FOV/2. FOV/3 and FOV/4 shifts between consecutive slices [3]

For simultaneously excited multi-slices, FOV/3 or FOV/4 shifts are desired. In that case, the period is 3 or 4 for k_y line dependent correction cycle. The blip schemes and phase diagrams describing the relative phase between the excited slices for different types of interslice shifts (FOV/2, FOV/3, FOV/4 shift) is shown in Fig. 13. It is necessary to give each slice a unique shift relative to the bottom slice for a coil without a z deviation in coil sensitivity patterns. For instance, 3 simultaneously excited slices, the shifts can be 0, FOV/3, and 2FOV/3. The aliased pixels can be separated in y. This pattern is shown in the FOV/3 diagram shown in Fig. 13. Similarly, when four slices are

simultaneously excited, and no z variation is existing in the coil array. If 5 slices are simultaneously excited and the array has some z variation, the FOV/4 shifts are suitable [3].

3.3 Slice-GRAPPA

In slice-GRAPPA algorithm, GRAPPA-like kernels are fit using prescan calibration data acquired from separately excited conventional single-slice data and then applies this kernel sets directly to the k-space data of the collapsed images. Thus, for the 2-fold slice-accelerated acquisition, two separate sets of GRAPPA kernels were fitted and applied, 1 for each imaging slice to generate each of the 2 imaging slices. This slice-GRAPPA algorithm is shown in Fig. 14. The appropriate equation for the algorithm is given below:

$$S_{j,z}(K_x,K_y) = \sum_{l=1}^{L} \sum_{b_x=-B_x}^{B_x} \sum_{b_{xy}=-B_y}^{B_y} n_{j,z,l}^{b_x,b} S_{l,collapse} \times (K_x - b_x \Delta K_x, K_y - b_y \Delta K_y) \qquad (20)$$

Here, for the slice located at z, $S_{j,z}(k_x,k_y)$ is the k-space data of the jth coil. $n_{j,z,l}^{bx,by}$ is the weight coefficient at location (b_x,b_y) in the GRAPPA kernel of the l'th coil. Thus, for a 32-channel coil, each of the 2 kernel sets (1 for each slice) is a set of 32 X 32 kernels (32 kernels to generate data for each of the 32 coil elements). The weight coefficient is applied on the collapsed data $S_{l,collapse}$ (k_x,k_y) to help create the missing data of the jth coil at slice location z.

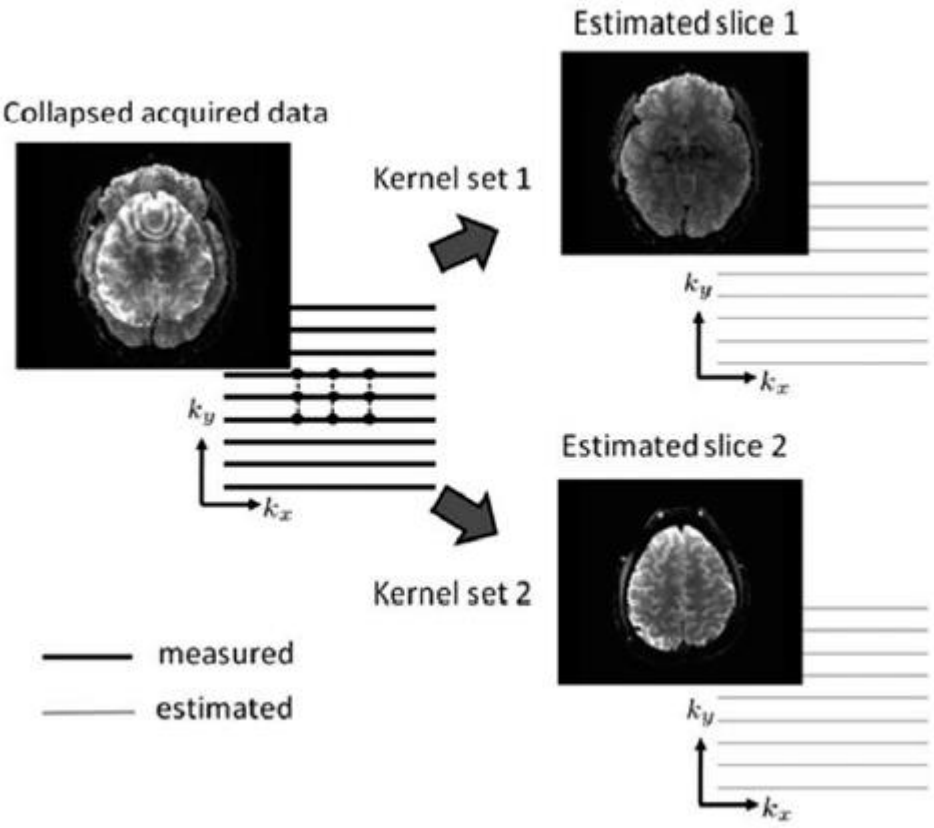

Figure 14: Slice-GRAPPA algorithm to acquire the k-space data for the unaliased slices. To synthesize k-space datasets for each slice, a set of GRAPPA kernels is used to the k-space data of the aliased slices. One kernel set is required for each slice [3]

Hence, slice-GRAPPA differs from conventional GRAPPA where the kernels work on the acquired k-space data to fill in missing lines. Rather the slice-GRAPPA kernels generate an entirely new set of k-space data for each coil of a given slice. For the multi-slice image acquisitions in addition with in-plane acceleration, the reconstructions methods were performed in successive steps. At first, the slice-GRAPPA was applied to isolate the aliased slices, then conventional GRAPPA was used to produce the missing k-space lines for the in-plane undersampled slices.

By expanding and simplifying (20), the governing equation for slice- GRAPPA can be obtained. The equation is given below:

$$C_{j,z}(x,y)\rho_z(x,y) = \sum_{l=1}^{L} C_{l,collapse}(x,y)\rho_{collapse}(x,y)K_{l,j,z}(x,y)$$

$$= \sum_{l=1}^{L}\{\sum_{sl=1}^{N_{slice}} C_{l,sl}(x,y)\rho sl(x,y)\}K_{l,j,z(x,y)}$$

$$= \sum_{sl=1}^{N_{slice}}\{\sum_{l=1}^{L} C_{l,sl}(x,y)K_{l,j,z}(x,y)\}\rho_{sl}(x,y) \quad (21)$$

Where $C_{j,z}(x,y)$ denotes the coil sensitivity profile of the j'th coil at slice location z;

ρ (x,y) is the underlying image of slice position z.;

$\rho_{collapse}(x,y)$ is the underlying image in the collapsed image.

For the case, when $N_{slice}=2$, this equation can be written as following:

$$C_{j,z}(x,y)\rho_z(x,y) = \{\sum_{l=1}^{L} C_{l,1}(x,y)K_{l,j,z}(x,y)\}\rho_1(x,y)+\{\sum_{l=1}^{L} C_{l,2}(x,y)K_{l,j,z}(x,y)\}\rho_2(x,y) \quad (22)$$

One thing to be noticed from (22) is that the resulting slice-GRAPPA kernels are dependent on the underlying images. This is different from conventional GRAPPA and has several consequences if this dependency is strong. Under typical imaging conditions, the governing equation can be simplified and written according to the following 2 equations where the dependence on the corresponding image no longer exist [3]:

$$C_{j,z}(x,y) = \sum_{l=1}^{L} C_{l,z}(x,y)K_{l,j,z}(x,y) \quad (23)$$

$$0 = \sum_{l=1}^{L} C_{l,sl}(x,y)K_{l,j,z}(x,y), for all sl \neq z \quad (24)$$

For the case, N_{slice} =2 and z =1, (23) and (24) satisfy (22) if the first term in (21) satisfies the equation and the second term is equal to zero. With these circumstances, the GRAPPA kernels are independent of the underlying images and are analogous to conventional GRAPPA, where the kernels are based solely on the relationships between the coil sensitivity patterns. The validity of (23) and (24) was tested for 2 simultaneous multi-slice acquisition [3].

3.4 Implementation

Modifications to the multi-slice parallel imaging technique have been used to lessen the high g-factor problem [3]. This blipped-controlled aliasing in parallel imaging for simultaneous multi-slice echo planar imaging method [3] was followed to reconstruct the image for the proposed stand-alone program . This method achieves spatial shifts in the PE direction between simultaneously excited multi-slices but avoids the voxel tilt problem in echo planar imaging [3]. This allows for application of image shifts in the PE direction to achieve great advantage in g-factor reduction. The method presents trivial loss of signal or blurring compared with the wideband or blipped-wideband methods [3].

In order to reconstruct the multi-slice image in the proposed stand-alone system, the raw data from the host computer is first corrected using the Orchestra software development kit by GE health-care [56] code written in C++. This C++ code removes the artifact by performing data whitening, Nyquist ghost correction, ramp sampling correction, Fermi filtering, notch filtering etc.

After the correction of raw data, the k-space data from simultaneously excited multi-slice is processed using the proposed C program. This proposed C code un-aliases the k-space data in the slice direction using the slice-GRAPPA algorithm. To accelerate the scan time, even faster if parallel imaging is used, the GRAPPA method is used in the proposed image reconstruction algorithm after applying slice-GRAPPA to calculate the missing k-space point in the phase encoding direction. An algorithm of this process is shown in Fig. 15.

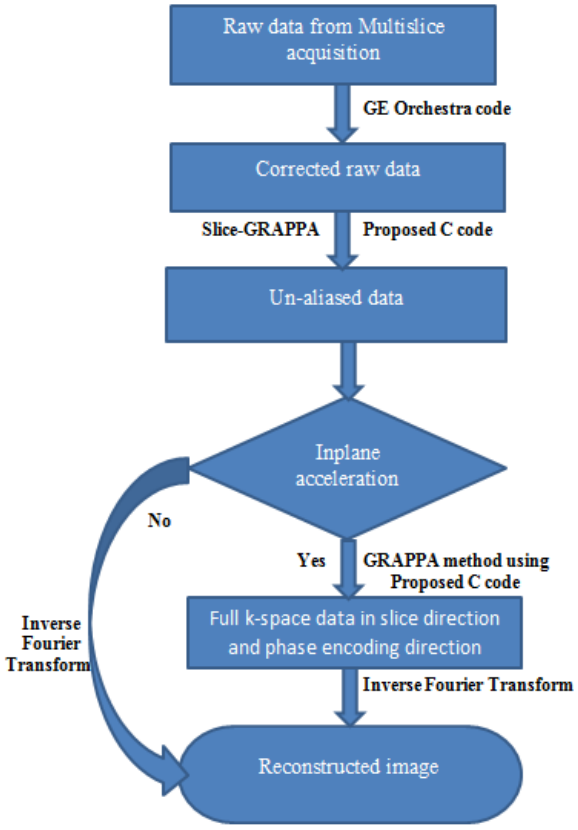

Figure 15: Algorithm for stand-alone, multi-slice EPI image reconstruction.

Chapter 4: Experiment and Results

The experiment was performed at the Laureate Institute for Brain Research (LIBR) with research protocol approved by the Western Institutional Review Board (IRB).

MRI images were acquired with a 3 Tesla MR scanner (GE MR750) using the multi-slice gradient-echo EPI sequence. The EPI imaging included the following parameters:

FOV = 24 cm

Matrix size = 96 x 96

TR/TE = 1000/30 ms

Flip angle = 90°

Total slices=48

Slice thickness = 2.5 mm

Slice acceleration (mux) = 3

In-plane acceleration (arc) = 1, 2

Image Volume=360

Voxel size=$2.5 \times 2.5 \times 2.5\ mm^3$

4.1 Results

The experimental result for the above-mentioned experiment with in-plane acceleration = 1 and slice acceleration = 3, for all slices at time point 14 is shown in the Fig. 16. The experimental result with in-plane acceleration = 2 and slice acceleration = 3 for all slices at time point 6 is shown in Fig. 17.

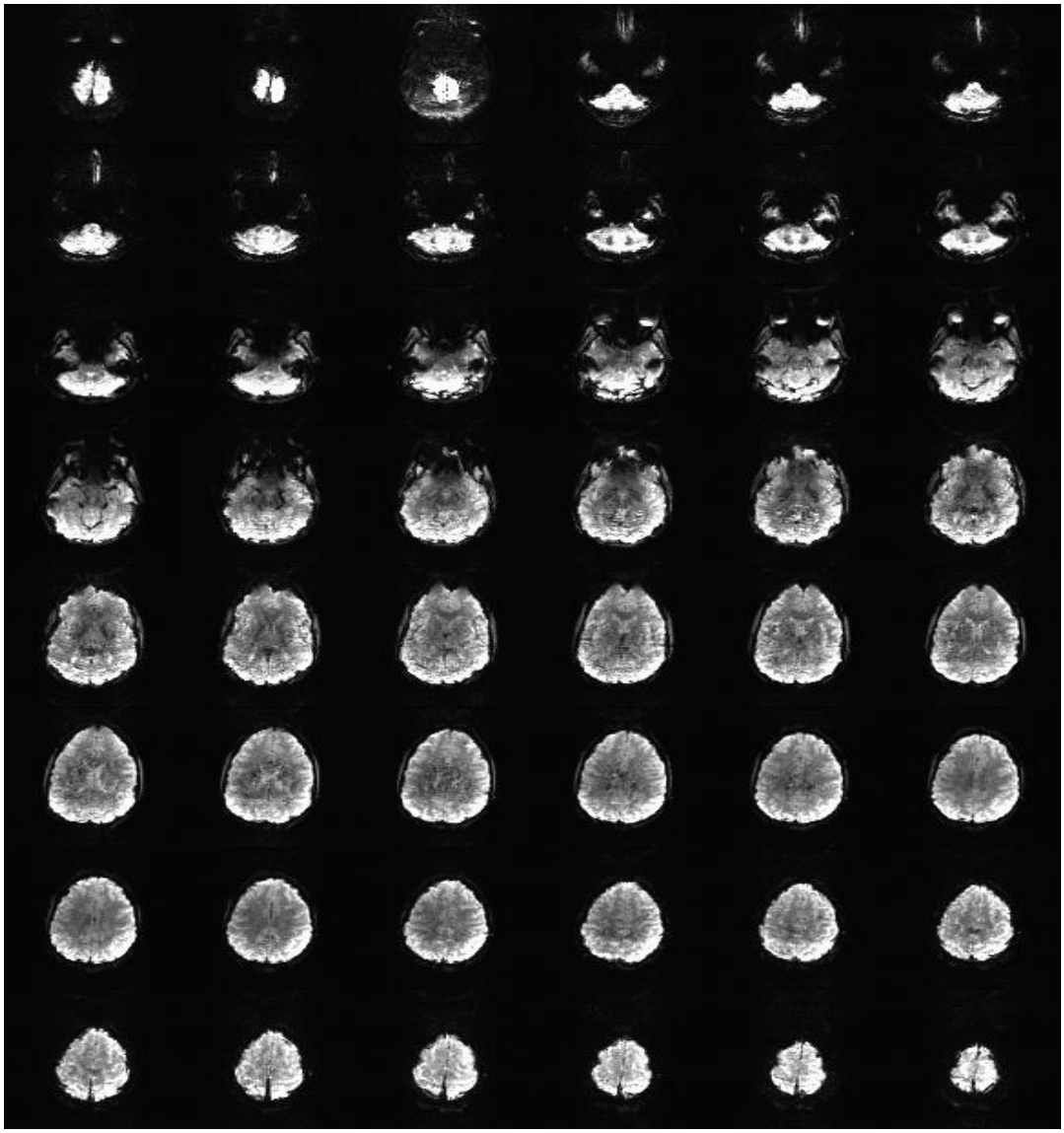

Figure 16: Image output from stand-alone multi-slice EPI image reconstruction system for 48 slices at a specific time point. Here, slice acceleration=3, in-plane acceleration=1

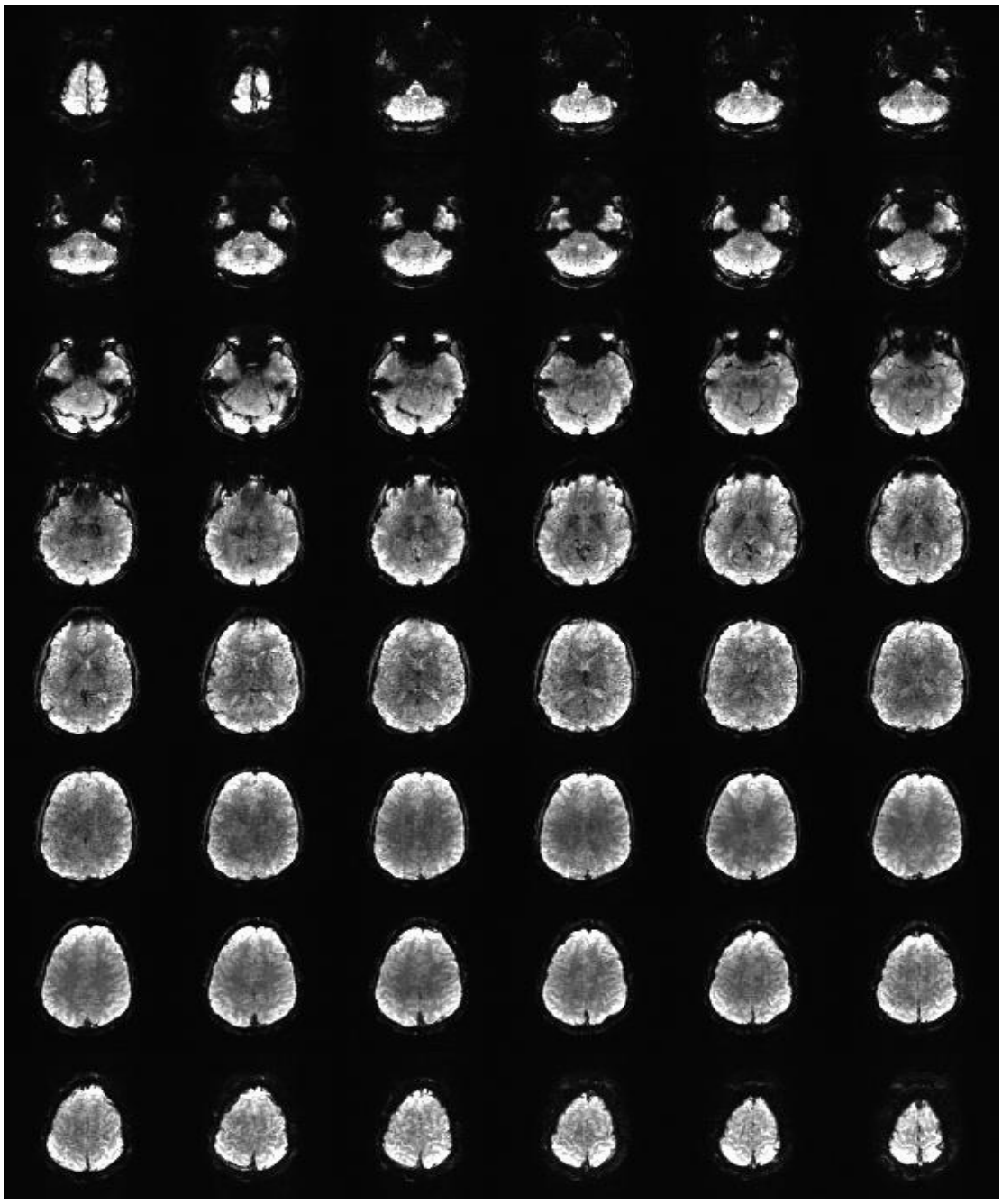

Figure 17: Image output from stand-alone multi-slice EPI image reconstruction system for 48 slices at a specific time point. Here, slice acceleration=3, in-plane acceleration=2

The same data was used in MATLAB to reconstruct the images to check the cross check of the images acquired from stand-alone reconstruction program shown inFig. 19. From Fig. 18 and Fig. 19, it can be concluded that both programs provide similar results. Thus, the results from stand-alone image reconstruction for multi-slice EPI are validated.

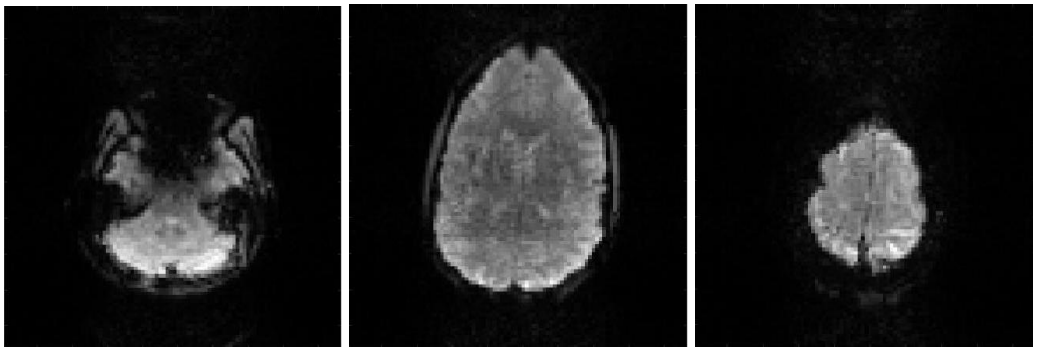

Figure 18: Image output from stand-alone multi-slice EPI image reconstruction system for 3 different slices at a specific time point. Here, slice acceleration=3, in-plane acceleration=1

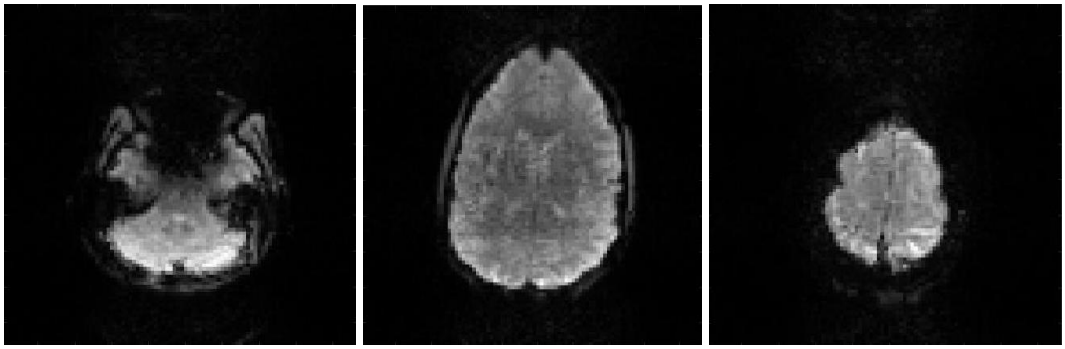

Figure 19: Image output from MATLAB program for same slices as acquired in stand-alone reconstruction program for slice acceleration=3, in-plane acceleration=1

Fig. 20 shows the reconstructed images from the stand-alone program for in-plane acceleration=2 and slice acceleration=3 for different slices at different time point.

Similarly, MATLAB software is used to reconstruct the images from simultaneously excited multi-slices which are shown in Fig. 21. Since the images from both reconstruction program is almost same, the proposed stand-alone reconstruction program is validated.

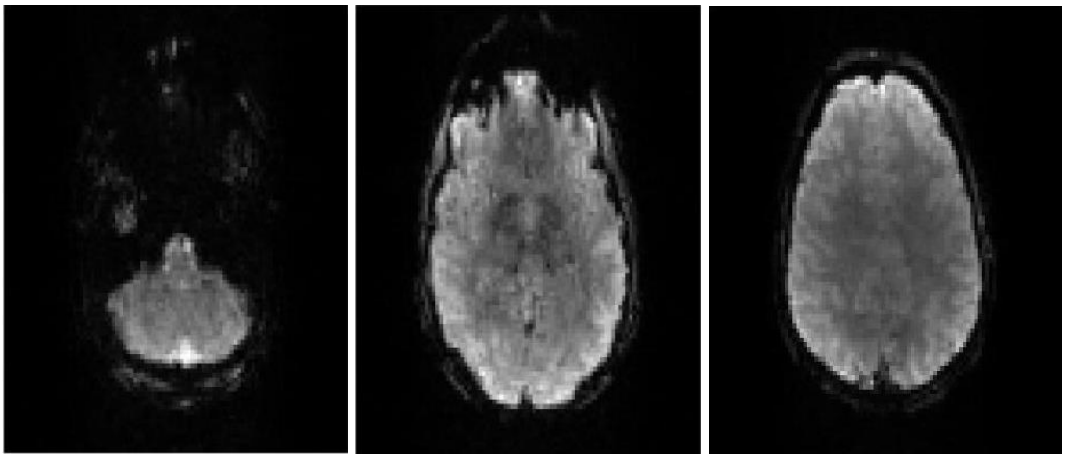

Figure 20: Image output from stand-alone multi-slice EPI image reconstruction system for 3 different slices at a specific time point. Here, slice acceleration=3, in-plane acceleration=2

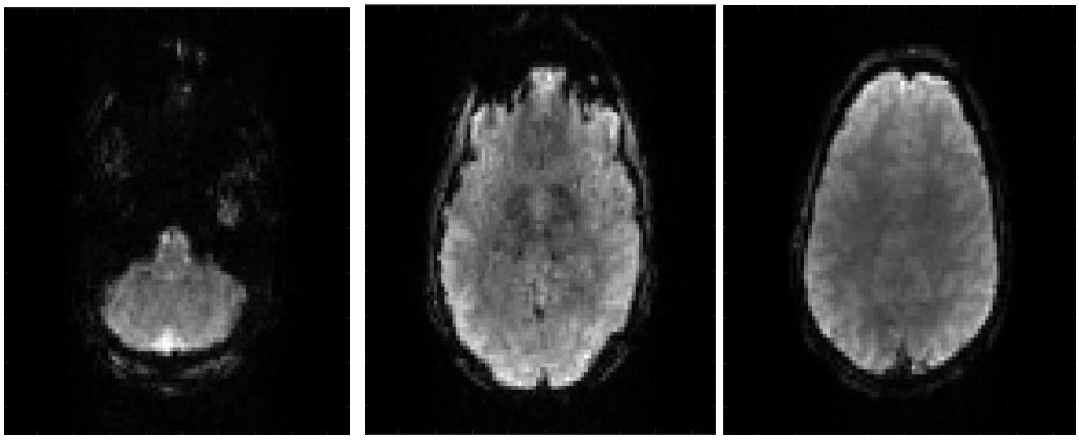

Figure 21: Image output from MATLAB program for same slices as acquired in stand-alone reconstruction program for slice acceleration=3, in-plane acceleration=2

Chapter 5: Conclusion

The research documented in this thesis concentrated on developing an image reconstruction program for multi-slice, echo-planar imaging that does not depend on the MATLAB environment. That program provides a great advantage for multi-slice, echo-planar-imaging reconstruction. This stand-alone reconstruction program is one step toward real-time implementation of code for multiband imaging. In order to implement it on real-time software, the speed of the reconstruction program needed to be faster. Although, the speed of the proposed stand-alone program is not fast enough to be implemented on real-time software, it can be optimized by paralleling the computation. Thus the real-time implementation of the proposed stand-alone code is promising and will allow for monitoring of subject motion and brain activation during scanning in order to adjust task presentation and for utilizing the brain signal to control other equipment and neurofeedback.

References

[1] Feinberg, David A., and Kawin Setsompop. "Ultra-fast MRI of the human brain with simultaneous multi-slice imaging." *Journal of magnetic resonance*229 (2013): 90-100.

[2] Guide, MATLAB User'S. "The mathworks." *Inc., Natick, MA* 5 (1998): 333.

[3] Setsompop, Kawin, et al. "Blipped-controlled aliasing in parallel imaging for simultaneous multislice echo planar imaging with reduced g-factor penalty."*Magnetic Resonance in Medicine* 67.5 (2012): 1210-1224.

[4] Griswold, Mark A., et al. "Generalized autocalibrating partially parallel acquisitions (GRAPPA)." *Magnetic resonance in medicine* 47.6 (2002): 1202-1210.

[5] [Online]. Available: http://www.scholarpedia.org/article/Magnetic_resonance_imaging.

[6] Heeger, David J., and David Ress. "What does fMRI tell us about neuronal activity?." *Nature Reviews Neuroscience* 3.2 (2002): 142-151.

[7] Logothetis, Nikos K., et al. "Neurophysiological investigation of the basis of the fMRI signal." *Nature* 412.6843 (2001): 150-157.

[8] Logothetis, Nikos K. "What we can do and what we cannot do with fMRI."*Nature* 453.7197 (2008): 869-878.

[9] Huettel, Scott A., Allen W. Song, and Gregory McCarthy. *Functional magnetic resonance imaging*. Vol. 1. Sunderland: Sinauer Associates, 2004.

[10] Huettel, Scott A., Allen W. Song, and Gregory McCarthy. *Functional magnetic resonance imaging*. Vol. 1. Sunderland: Sinauer Associates, 2004.

[11] [Online]. Available: http://www.ndcn.ox.ac.uk/divisions/fmrib/what-is-fmri/introduction-to-fmri

[12] Peters, Andrew M., et al. "T 2* measurements in human brain at 1.5, 3 and 7 T." *Magnetic resonance imaging* 25.6 (2007): 748-753.

[13] Narsude, Mayur. "High Temporal Resolution Functional Magnetic Resonance Imaging at 7 Tesla." (2014).

[14] Chapman, B., et al. "Real-time movie imaging from a single cardiac cycle by NMR." *Magnetic resonance in medicine* 5.3 (1987): 246-254.

[15] Giannelli, Marco, et al. "Characterization of Nyquist ghost in EPI-fMRI acquisition sequences implemented on two clinical 1.5 T MR scanner systems: effect of readout bandwidth and echo spacing." *Journal of Applied Clinical Medical Physics* 11.4 (2010).

[16] Cohen, Mark S. "Echo-planar imaging (EPI) and functional MRI." *Functional MRI, Springer Verlag, Berlin* (1999).

[17] Bernstein, Matt A., Kevin F. King, and Xiaohong Joe Zhou. *Handbook of MRI pulse sequences*. Elsevier, 2004.

[18] Hahn, Erwin L. "Spin echoes." *Physical review* 80.4 (1950): 580.

[19] [Online]. Available: http://www.xrayphysics.com/sequences.html

[20] Deshmane, Anagha, et al. "Parallel MR imaging." *Journal of Magnetic Resonance Imaging* 36.1 (2012): 55-72.

[21] Cohen, Mark S., et al. "Sensory stimulation by time-varying magnetic fields."*Magnetic resonance in medicine* 14.2 (1990): 409-414.

[22] Ham, C. L. G., et al. "Peripheral nerve stimulation during MRI: effects of high gradient amplitudes and switching rates." *Journal of Magnetic Resonance Imaging* 7.5 (1997): 933-937.

[23] Hoffmann, A., et al. "Electromyography in MRI—first recordings of peripheral nerve activation caused by fast magnetic field gradients." *Magnetic resonance in medicine* 43.4 (2000): 534-539.

[24] Hoult, D. I., C-N. Chen, and V. J. Sank. "The field dependence of NMR imaging. II. Arguments concerning an optimal field strength." *Magnetic resonance in medicine* 3.5 (1986): 730-746.

[25] Roemer, Peter B., et al. "The NMR phased array." *Magnetic resonance in medicine* 16.2 (1990): 192-225.

[26] Walsh, David O., Arthur F. Gmitro, and Michael W. Marcellin. "Adaptive reconstruction of phased array MR imagery." *Magnetic Resonance in Medicine* 43.5 (2000): 682-690.

[27] Pruessmann, Klaas P., et al. "SENSE: sensitivity encoding for fast MRI."*Magnetic resonance in medicine* 42.5 (1999): 952-962.

[28] Blaimer, Martin, et al. "SMASH, SENSE, PILS, GRAPPA: how to choose the optimal method." *Topics in Magnetic Resonance Imaging* 15.4 (2004): 223-236.

[29] Sodickson, Daniel K., and Warren J. Manning. "Simultaneous acquisition of spatial harmonics (SMASH): fast imaging with radiofrequency coil arrays."*Magnetic Resonance in Medicine* 38.4 (1997): 591-603.

[30] Jakob, Peter M., et al. "AUTO-SMASH: a self-calibrating technique for SMASH imaging." *Magnetic Resonance Materials in Physics, Biology and Medicine* 7.1 (1998): 42-54.

[31] Heidemann, Robin M., et al. "VD-AUTO-SMASH imaging." *Magnetic Resonance in Medicine* 45.6 (2001): 1066-1074.

[32] Ahmed, Haitham Mohamed Ahmed. "Reconstruction techniques in parallel magnetic resonance imaging." (2010).

[33] McKenzie, Charles A., et al. "Self-calibrating parallel imaging with automatic coil sensitivity extraction." *Magnetic Resonance in Medicine* 47.3 (2002): 529-538.

[34] Roemer, Peter B., et al. "The NMR phased array." *Magnetic resonance in medicine* 16.2 (1990): 192-225.

[35] Walsh, David O., Arthur F. Gmitro, and Michael W. Marcellin. "Adaptive reconstruction of phased array MR imagery." *Magnetic Resonance in Medicine* 43.5 (2000): 682-690.

[36] Goldfarb, James W. "The SENSE ghost: Field-of-view restrictions for SENSE imaging." *Journal of Magnetic Resonance Imaging* 20.6 (2004): 1046-1051.

[37] Griswold, Mark A., et al. "Field-of-view limitations in parallel imaging."*Magnetic resonance in medicine* 52.5 (2004): 1118-1126.

[38] Pruessmann, Klaas P., et al. "SENSE: sensitivity encoding for fast MRI."*Magnetic resonance in medicine* 42.5 (1999): 952-962.

[39] Larkman, David J., et al. "Use of multicoil arrays for separation of signal from multiple slices simultaneously excited." *Journal of Magnetic Resonance Imaging* 13.2 (2001): 313-317.

[40] Sharma, Anuj. *Radiofrequency Pulses For Improved Simultaneous Multislice Magnetic Resonance Imaging*. Diss. Vanderbilt University, 2015.

[41] Blaimer, Martin, et al. "Accelerated volumetric MRI with a SENSE/GRAPPA combination." *Journal of Magnetic Resonance Imaging* 24.2 (2006): 444-450.

[42] Lindquist, Martin A., et al. "Rapid three-dimensional functional magnetic resonance imaging of the initial negative BOLD response." *Journal of Magnetic Resonance* 191.1 (2008): 100-111.

[43] Mansfield, Peter, Ronald Coxon, and Jonathan Hykin. "Echo-volumar imaging (EVI) of the brain at 3.0 T: first normal volunteer and functional imaging results." *Journal of computer assisted tomography* 19.6 (1995): 847-852.

[44] van der Zwaag, Wietske, Susan Francis, and Richard Bowtell. "Improved echo volumar imaging (EVI) for functional MRI." *Magnetic resonance in medicine* 56.6 (2006): 1320-1327.

[45] Rabrait, Cecile, et al. "High temporal resolution functional MRI using parallel echo volumar imaging." *Journal of Magnetic Resonance Imaging* 27.4 (2008): 744-753.

[46] Witzel, T., et al. "Single-shot echo-volumar imaging using highly parallel detection." *Proc ISMRM*. Vol. 1387. 2008.

[47] Weaver, John B. "Simultaneous multislice acquisition of MR images."*Magnetic resonance in medicine* 8.3 (1988): 275-284.

[48] Paley, Martyn NJ, et al. "Simultaneous parallel inclined readout image technique." *Magnetic resonance imaging* 24.5 (2006): 557-562.

[49] Wu, E. L., J. H. Chen, and T. D. Chiueh. "Wideband MRI: A new dimension of MR image acceleration." *Proceedings of the 17th Annual Meeting of ISMRM*. 2009.

[50] Feinberg, David A., Timothy G. Reese, and Van J. Wedeen. "Simultaneous echo refocusing in EPI." *Magnetic resonance in medicine* 48.1 (2002): 1-5.

[51] Reese, Timothy G., et al. "Halving imaging time of whole brain diffusion spectrum imaging and diffusion tractography using simultaneous image refocusing in EPI." *Journal of Magnetic Resonance Imaging* 29.3 (2009): 517-522.

[52] Larkman, David J., et al. "Use of multicoil arrays for separation of signal from multiple slices simultaneously excited." *Journal of Magnetic Resonance Imaging* 13.2 (2001): 313-317.

[53] Breuer, Felix A., et al. "Controlled aliasing in parallel imaging results in higher acceleration (CAIPIRINHA) for multi-slice imaging." *Magnetic resonance in medicine* 53.3 (2005): 684-691.

[54] Nunes, R. G., et al. "Simultaneous slice excitation and reconstruction for single shot EPI." *Proceedings of the 14th annual meeting of ISMRM, Seattle, Washington, USA*. 2006.

[55] Moeller, Steen, et al. "Multiband multislice GE-EPI at 7 tesla, with 16-fold acceleration using partial parallel imaging with application to high spatial and temporal whole-brain fMRI." *Magnetic Resonance in Medicine* 63.5 (2010): 1144-1153.

[56] GE Healthcare. http://www.gehealthcare.com/